doi:10.1038/nature12347

1. Supplementary Figures

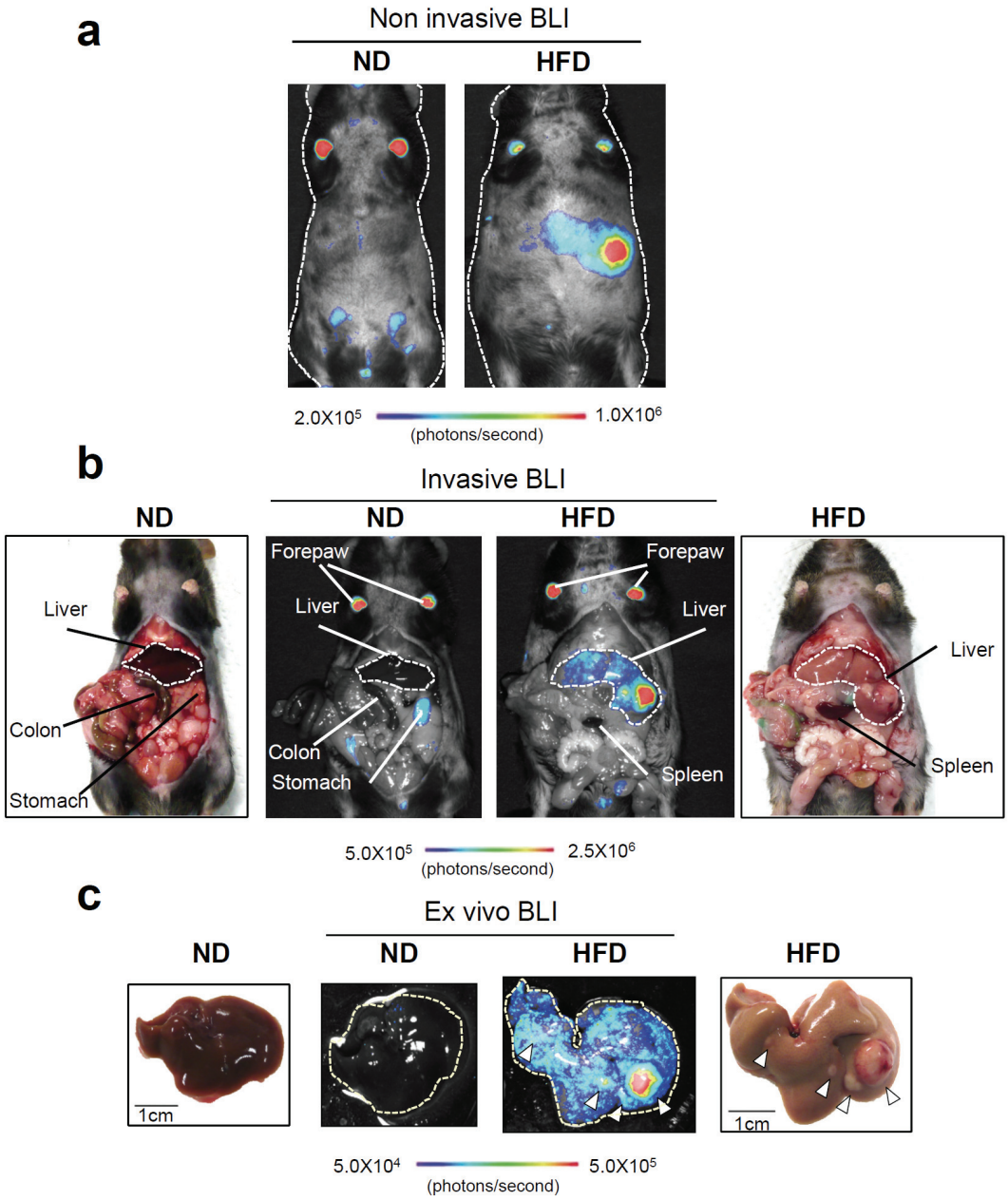

Supplementary Fig. 1 | *In vivo* imaging of p21$^{Waf1/Cip1}$ expression.
a, Neonatal p21-*p*-luc mice (C57BL/6) were treated with DMBA, and then fed either ND (left) or HFD (right) for 30 weeks (see Fig.1a). Real-time non-invasive BLI of p21-*p*-luc mice was performed. Representative images of two independent experiments are shown. The colour bar indicates photons with minimum and maximum threshold values. **b,** The mice used in panel a were incised through the mouth and anus under

anaesthesia and were subjected to invasive BLI. Representative images of two independent experiments are shown. **c,** The mice used in panel b were sacrificed and livers were rapidly removed and placed in culture dishes, and *ex vivo* BLI was performed. Macroscopic photographs of livers are also shown. The arrowheads indicate HCC. The colour bar indicates photons with minimum and maximum threshold values.

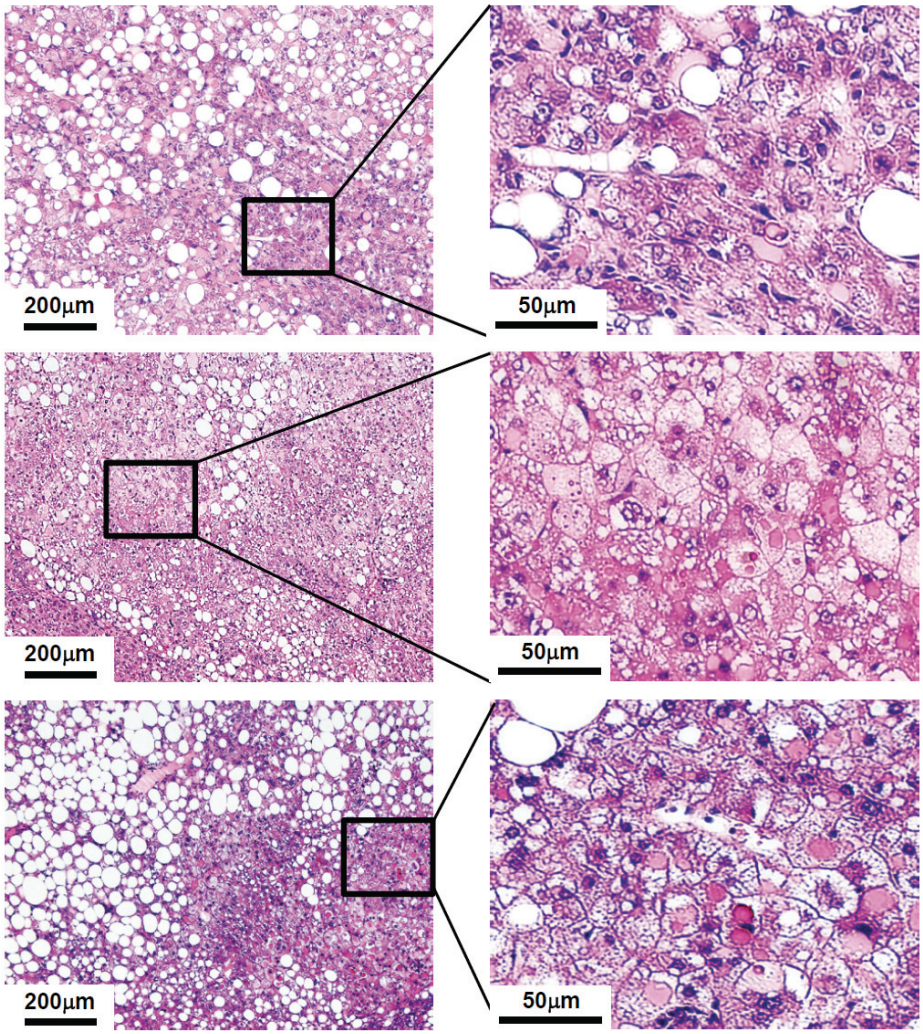

Supplementary Fig. 2 | Histopathology of liver cancer. The neonatal WT (C57BL/6) mice were treated with a single application of DMBA at neonatal stage, and then fed HFD for 30 weeks (see Fig.1a). Liver sections of tumour regions were subjected to H&E staining and representative images were shown. These tumours were diagnosed as hepatocellular carcinoma (HCC) with marked fatty change and intracytoplasmic body. Fibrosis was not apparent. These tumours resembled human HCC (see Supplementary Fig.15).

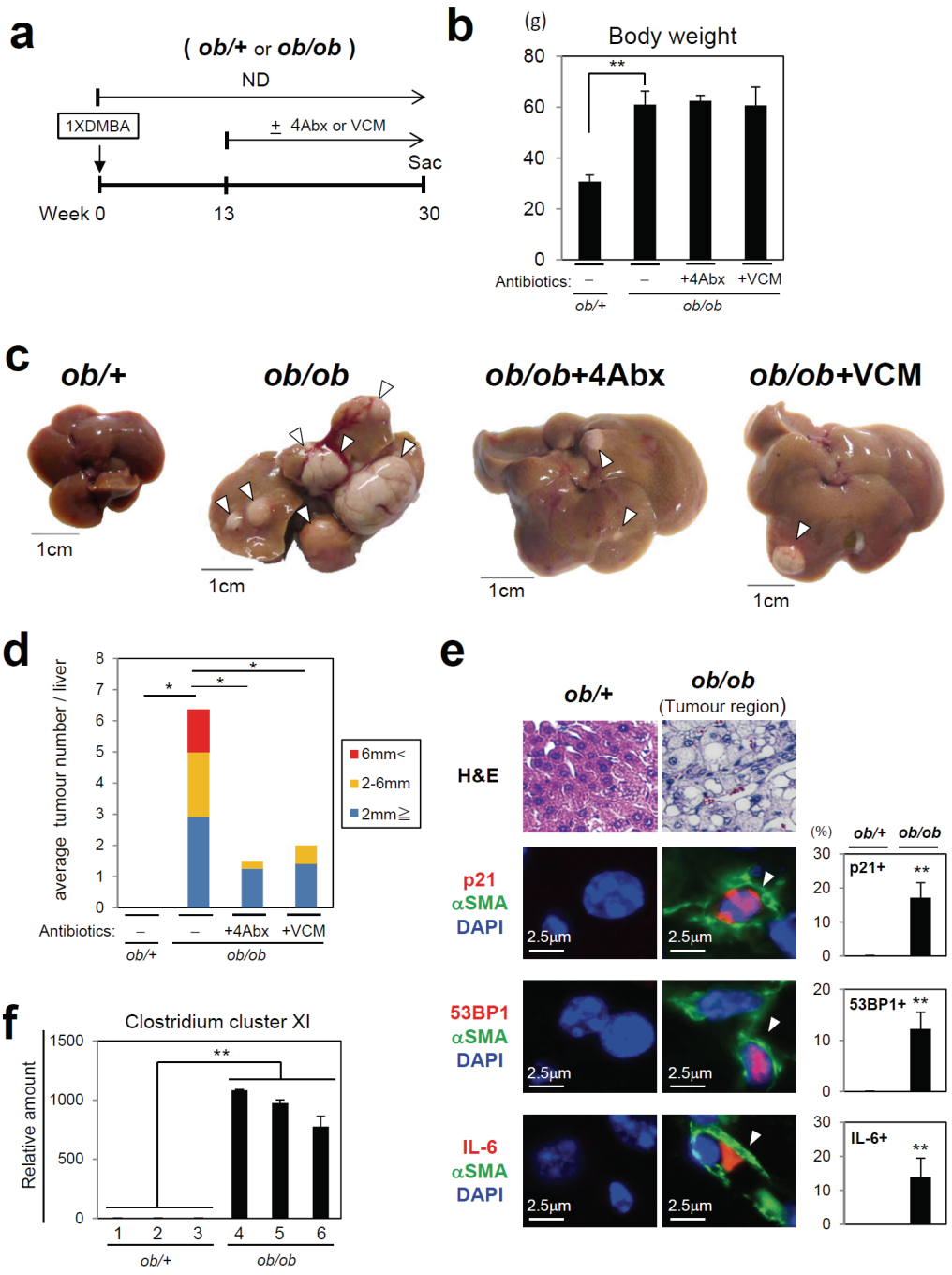

Supplementary Fig. 3 | *ob/ob* mice developed DMBA-induced liver cancer. **a,** Timeline of the experimental procedure (*ob/+* : n=7, *ob/ob* : n=11, *ob/ob* with combination of four antibiotics (4Abx) : n=4, and *ob/ob* mice with vancomycin (VCM) : n=5). **b,** The average body weights of the indicated mice at the age of 30 weeks. **c,** Representative macroscopic photographs of livers from the indicated mice are shown. **d,** The average tumour numbers and their relative size distribution (classified as 6mm< , 2-6mm, and 2mm≧) of indicated mice. **e,** Immunofluorescence analysis of

liver sections from the indicated mice were performed using antibodies shown left. The histograms on the right of the micrographs indicate the percentages of α-SMA expressing cells that were positive for the indicated markers. HSCs were visualized by α-SMA and DNA was stained by DAPI. At least 100 cells were scored per group. **f,** The quantitative real time PCR (qPCR) analysis of *Clostridium* cluster XI 16S rRNA gene in the feces (180mg) of the indicated mice (n=3 per group). For all graphs, error bars indicate mean ± s.d. **P*<0.05, ***P*<0.01.

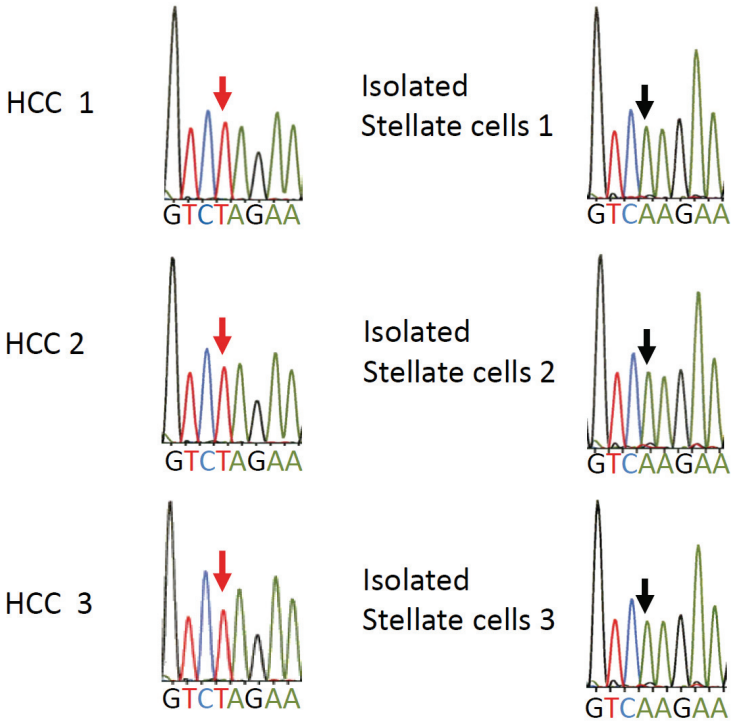

Supplementary Fig. 4| Detection of oncogenic mutation (A to T change at codon 61) in *H-ras* gene. We examined the oncogenic *ras* mutation in HCCs and HSCs isolated from tumour regions. As shown in the figure above, although the oncogenic *ras* mutation was clearly detected in all of the HCCs we tested, this was not the case in HSCs, indicating that the oncogenic *ras* mutation in HSCs is not a prerequisite for the observed phenotypes.

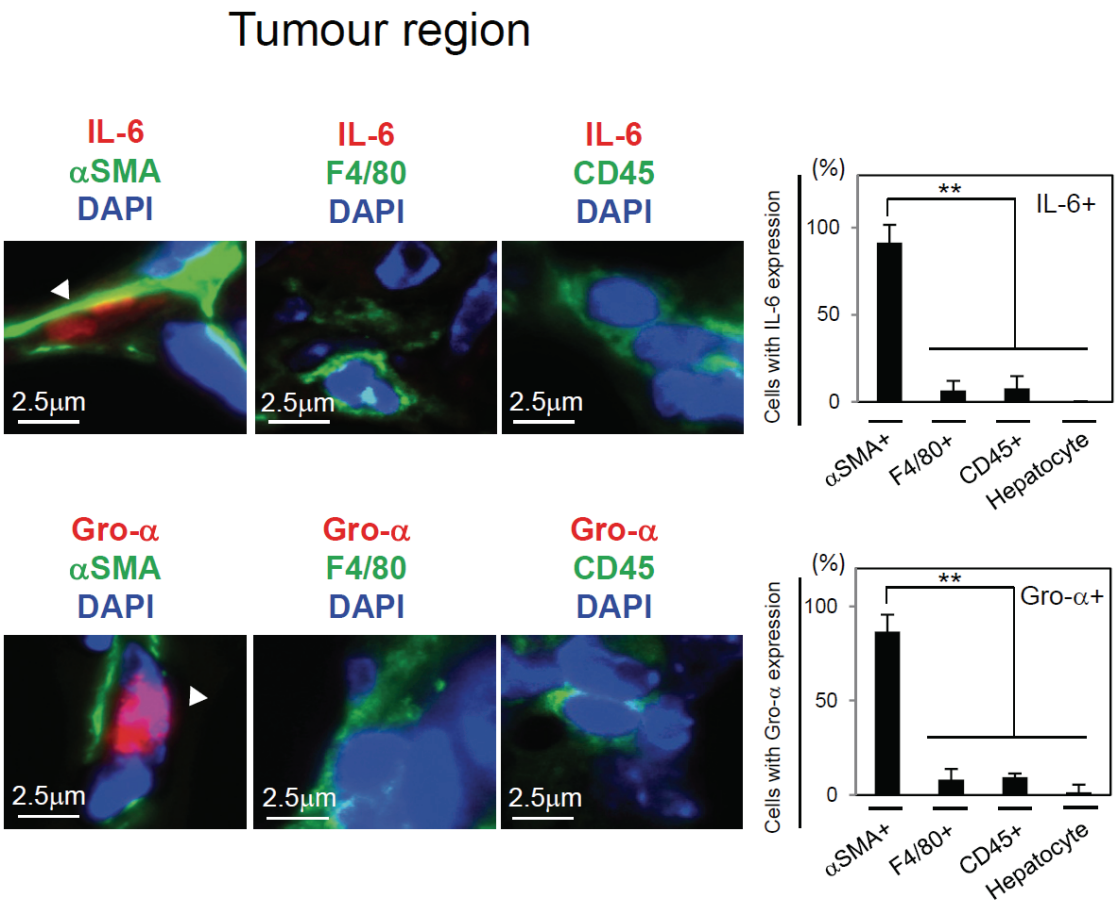

Supplementary Fig. 5| SASP factor expression in liver cells.
Sections of obesity-associated liver tumours (see Fig. 1f, HFD) were subjected to immunofluorescence analysis using the antibodies shown top. Histograms on the right side of the micrographs indicate the percentage of α-SMA positive cells, F4/80 positive cells, CD45 positive cells and Hepatocytes (Hep) with IL-6 expression (upper panel) or Gro-α expression (lower panel). At least 100 cells were scored per group. The data are shown as means ± s.d. and are representative of three independent experiments (n=3 per group). $^{**}P<0.01$.

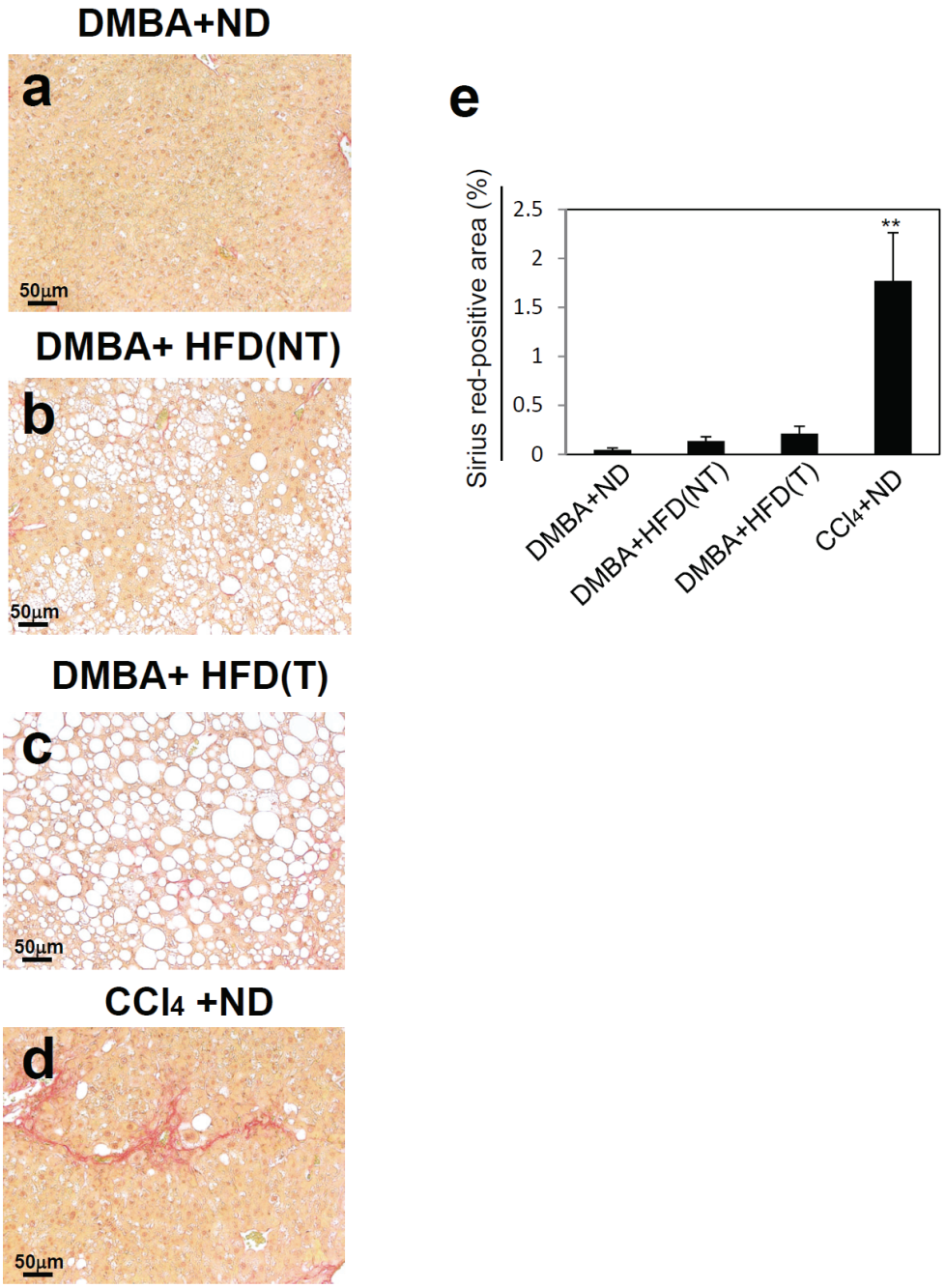

Supplementary Fig. 6| Lack of fibrosis development in the liver of neonatal DMBA plus HFD-induced HCC model. **a-c**, Neonatal WT mice were treated with DMBA, and then fed either ND (a) or HFD (b and c) for 30 weeks. **d,** Eight week old WT mice were treated with CCl_4 for 6 weeks. Paraffin-embedded liver sections were stained with Sirius Red (a-d). At least three whole sections from each mouse were scanned by Laser Scanner Cytometry for fibrosis quantification as reported previously[11]. **e**, These images were quantified using NIH Image J software. The data are shown as means ± s.d. $^{**}P<0.01$. (NT): non-tumour region. (T): tumour region. (n=10 per group)

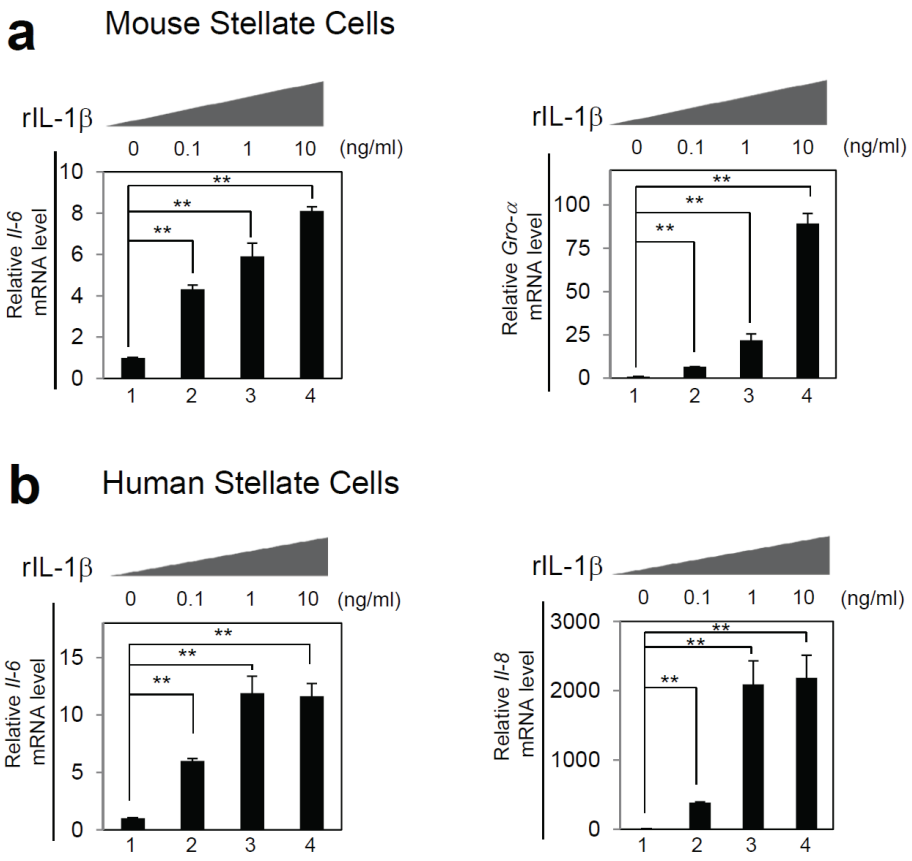

Supplementary Fig. 7| Dose dependent induction of *Il-6* and *Gro-α (Il-8)* mRNA by recombinant IL-1β treatment. **a,** Recombinant IL-1β was purchased from MACS Miltenyi biotec, inc, and was added to murine primary HSCs as following doses: lane 1 (0ng/ml), lane 2 (0.1ng/ml), lane 3 (1.0 ng/ml), lane 4 (10.0ng/ml). RNA was then prepared from these cells and was subjected to analysis of RT-qPCR for *Il-6* or *Gro-α* (a functional homologue of human *Il-8*) genes. **b,** Recombinant IL-1β was added to human primary HSCs as following doses: lane 1 (0ng/ml), lane 2 (0.1ng/ml), lane 3 (1.0 ng/ml), lane 4 (10.0ng/ml). RNA was then prepared from these cells and was subjected to analysis of RT-qPCR for *Il-6* or *Il-8* genes. For all graphs, error bars indicate mean ± s.d. of triplicate measurements. ***P*<0.01. Representative data from two independent experiments are shown.

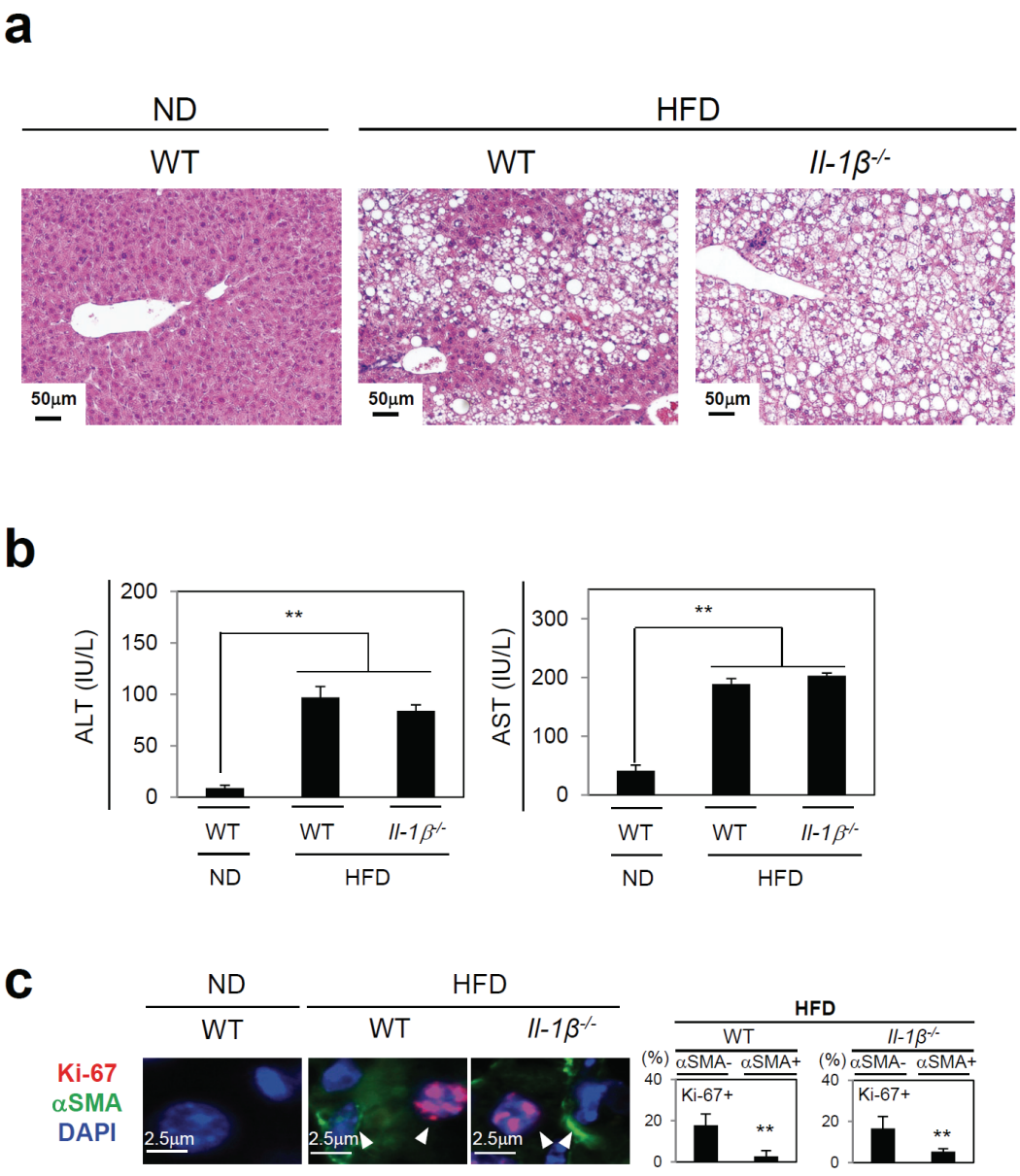

Supplementary Fig. 8| The degree of steatohepatitis was not attenuated in *Il-1β* knockout mice. **a,** Liver sections of the indicated mice (see Fig.2 a) were subjected to H&E staining and representative images of each group were shown. **b,** Serum alanine amino-transferase (ALT) and aspartate amino-transferase (AST) levels in indicated mice were determined. **c,** Immunofluorescence analysis of liver sections from the indicated mice were performed using antibodies shown left. The histograms on the right of the micrographs indicate the percentages of α-SMA positive (+) or negative (-) cells with Ki-67 expression. HSCs were visualized by α-SMA and DNA was stained by DAPI. The scale bars represent 2.5μm. For all graphs, error bars indicate mean ± s.d. (ND-WT: n=19, HFD-WT: n=19, HFD-*Il-1β*$^{-/-}$: n=9). ***P*<0.01.

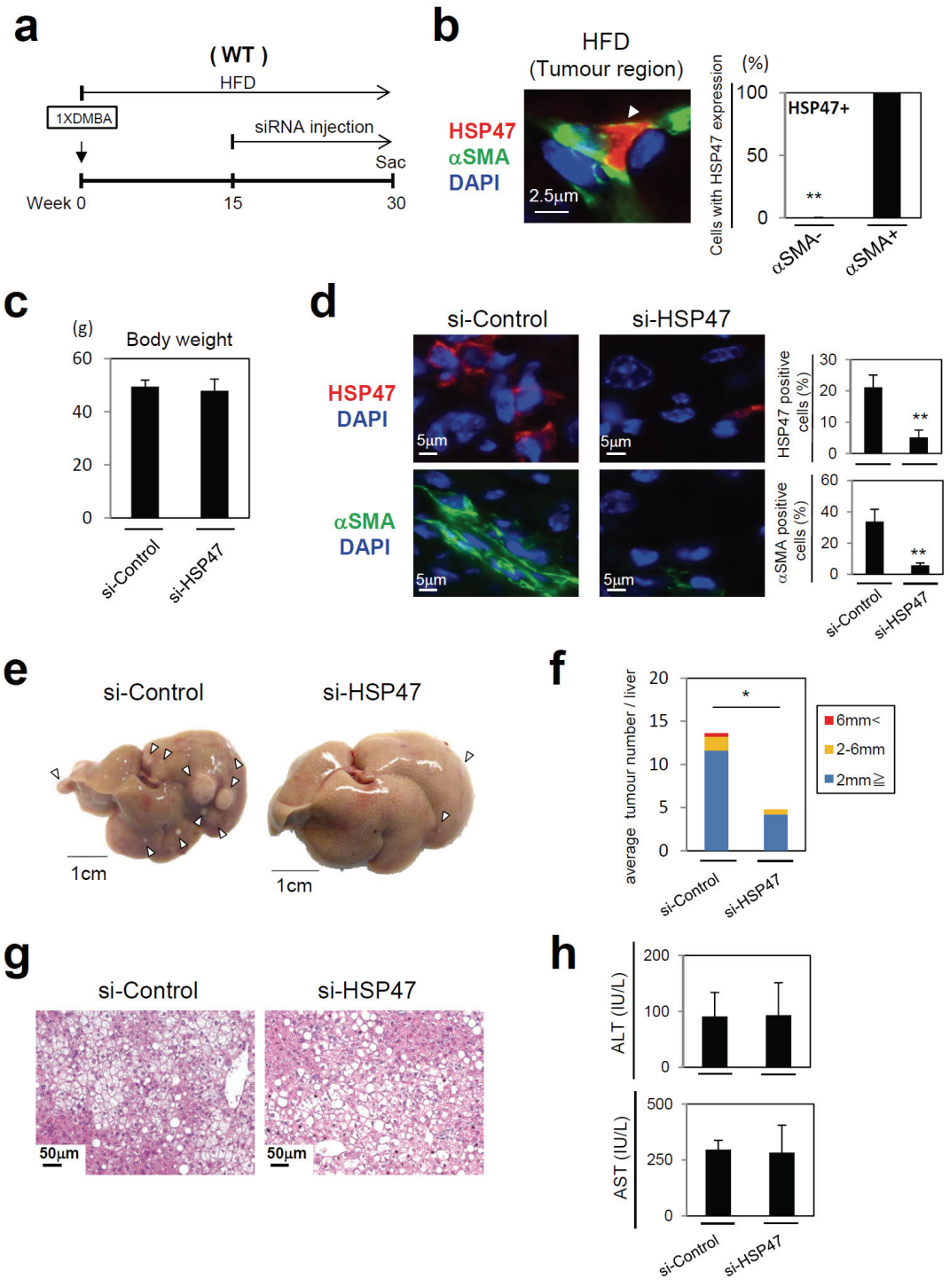

Supplementary Fig. 9| *In vivo* knockdown of HSP47 causes a decrease of activated HSCs abundance and reduction of HCC development in obese mice. **a,** Timeline of the experimental procedure (n=5 per group). The siRNA against control or HSP47 was intravenously injected with an amount of 3μg/g (weight) through mice's tail vein twice a week for 15weeks. **b,** Sections of obesity-associated liver tumours (HFD) were

subjected to immunofluorescence analysis using the antibodies shown left. Histograms on the right side of the micrographs indicate the percentage of α-SMA positive (+) or negative (-) cells with HSP47 expression. **c,** The average body weights at the age of 30weeks. **d,** Immunofluorescence analysis of liver sections from the indicated mice were performed using the antibodies shown left. The histograms on the right of the micrographs indicate the percentages of cells that were positive for the indicated markers. DNA was stained by DAPI. At least 100 cells were scored per group. **e,** Representative macroscopic photographs of livers from mice injected with siRNA against control (left) or HSP47 (right). **f,** The average tumour numbers and their relative size distribution (classified as 6mm< , 2-6mm, and 2mm≧) of indicated mice. **g,** Liver sections of the indicated mice were subjected to H&E staining and representative images of each group were shown. **h,** Serum alanine amino-transferase (ALT) and aspartate amino-transferase (AST) levels in indicated mice were determined. For all graphs, error bars indicate mean ± s.d. $*P<0.05, **P<0.01$.

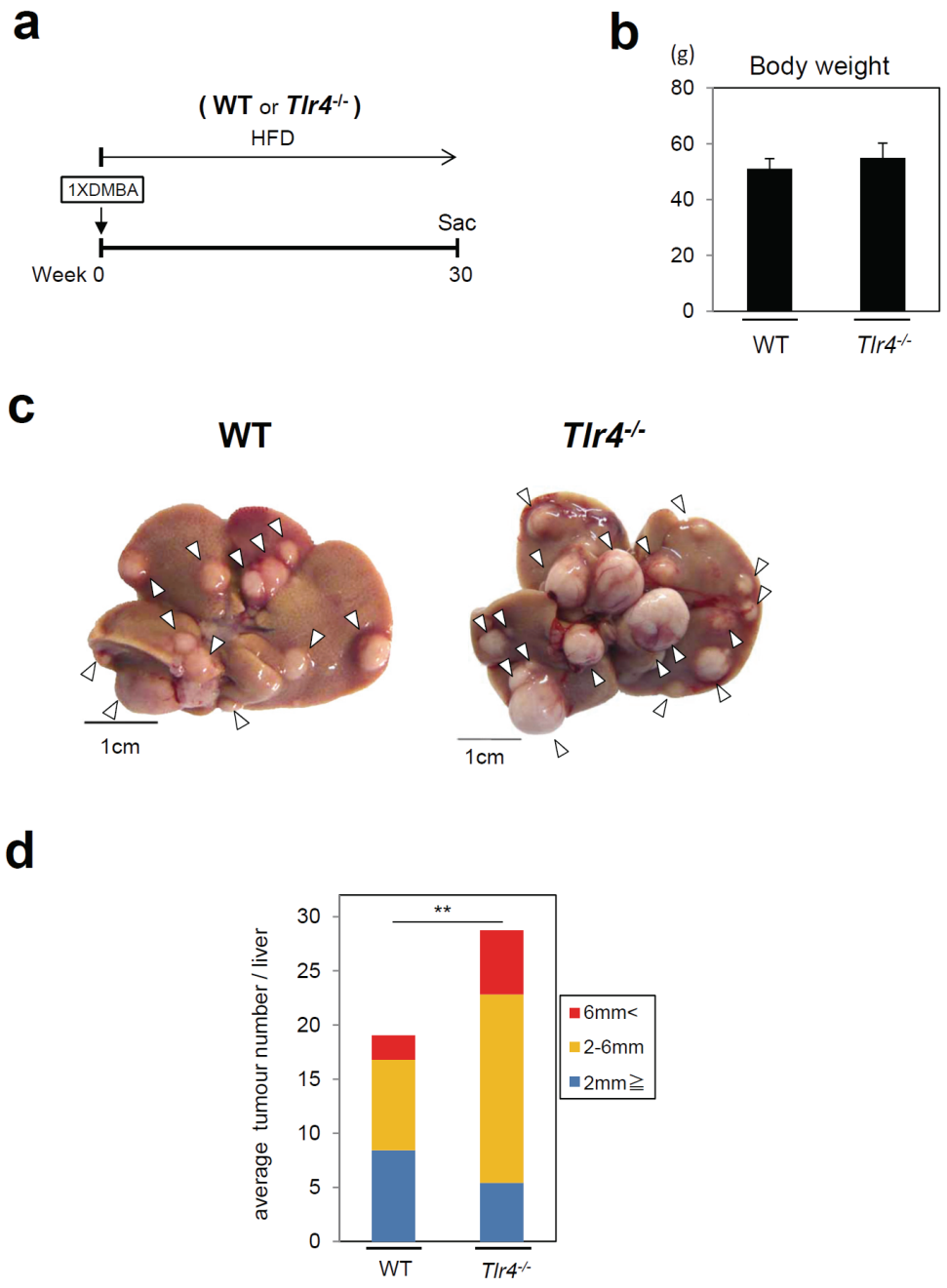

Supplementary Fig. 10| TLR4 deficiency promotes HFD-induced HCC development. **a,** Timeline of the experimental procedure (WT : n=19, *Tlr4*$^{-/-}$: n=12). **b,** The average body weights at the age of 30weeks. **c,** Representative macroscopic photographs of livers from WT (left) or TLR4 deficient (right) mice. **d,** The average tumour numbers and their relative size distribution (classified as 6mm< , 2-6mm, and 2mm≧) of the indicated mice. For all graphs, error bars indicate mean ± s.d. ***P*<0.01.

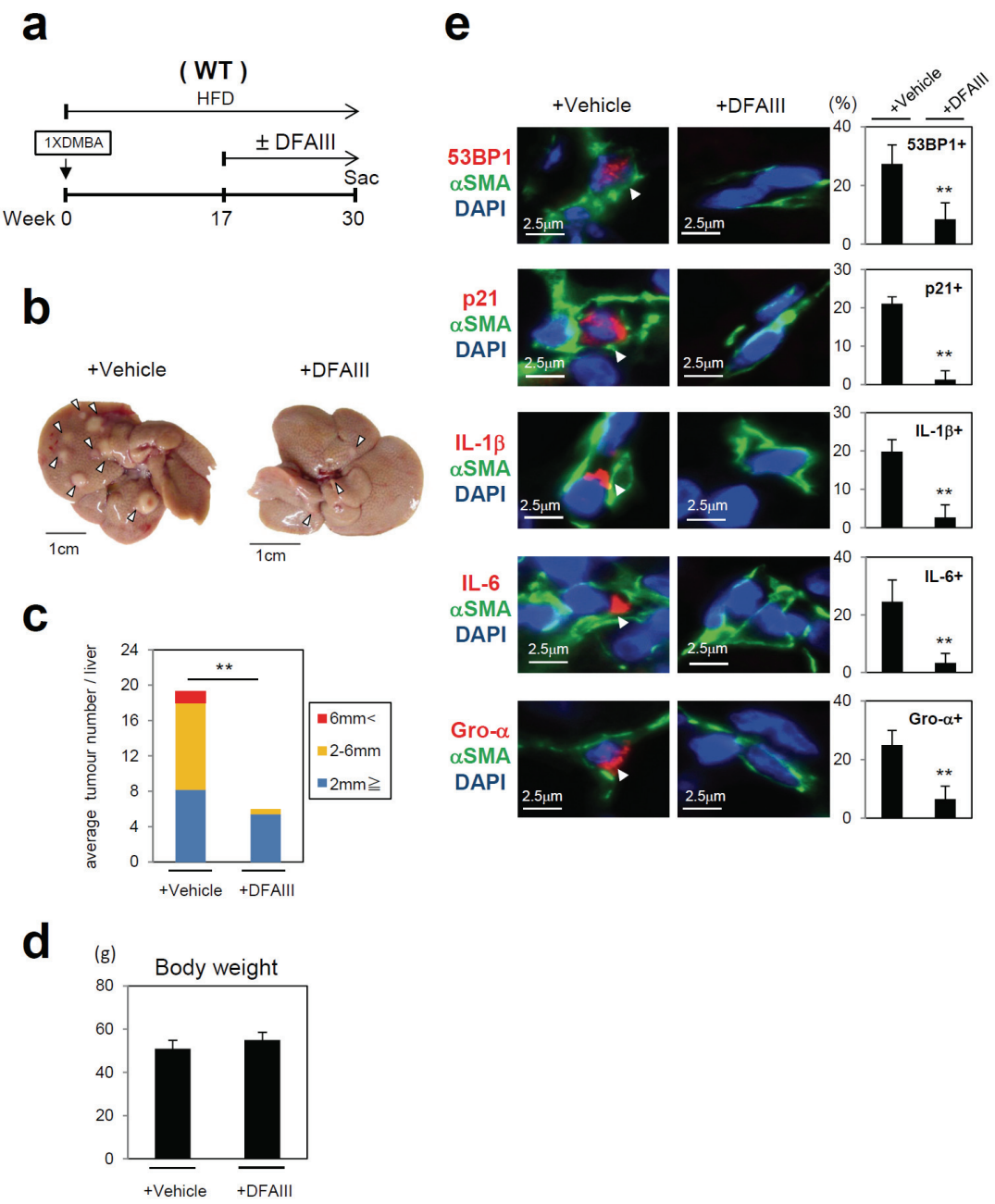

Supplementary Fig. 11| DFAIII alleviates obesity-induced HCC development. **a,** Timeline of the experimental procedure (+Vehicle: n=6, +DFAIII: n=5). **b,** Representative macroscopic photographs of livers from mice treated with vehicle (left) or DFAIII (right). **c,** The average tumour numbers and their relative size distribution (classified as 6mm< , 2-6mm, and 2mm≧) of the indicated mice. **d,** The average body weight at the age of 30weeks. **e,** Immunofluorescence analysis of liver section from the indicated mice were performed using the antibodies shown left. The histograms on the right of the micrographs indicate the percentages of α-SMA expressing cells that were

positive for the indicated markers. HSCs were visualized by α-SMA and DNA was stained by DAPI. At least 100 cells were scored per group. For all graphs, error bars indicate mean ± s.d. **P<0.01.

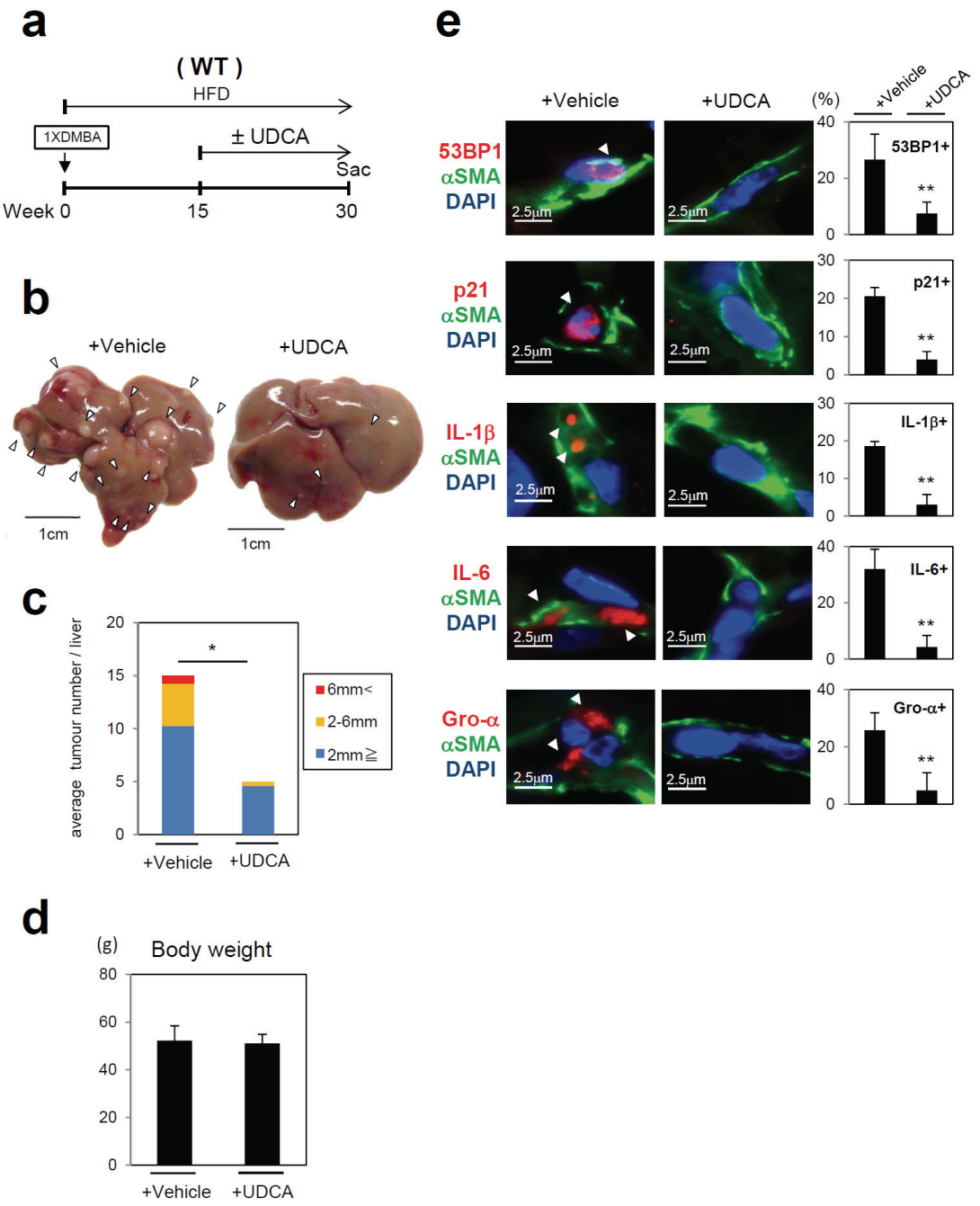

Supplementary Fig. 12| UDCA alleviates obesity-induced HCC development. **a,** Timeline of the experimental procedure (+Vehicle: n=4, +UDCA: n=5). **b,** Representative macroscopic photographs of livers from mice treated with vehicle (left)

or UDCA (right). **c,** The average tumour numbers and their relative size distribution (classified as 6mm< , 2-6mm, and 2mm≧) of the indicated mice. **d,** The average body weights at the age of 30weeks. **e,** Immunofluorescence analysis of liver section from the indicated mice were performed using the antibodies shown left. The histograms on the right of the micrographs indicate the percentage of α-SMA expressing cells that were positive for the indicated markers. HSCs were visualized by α-SMA and DNA was stained by DAPI. At least 100 cells were scored per group. For all graphs, error bars indicate mean ± s.d. **P*<0.05,***P*<0.01.

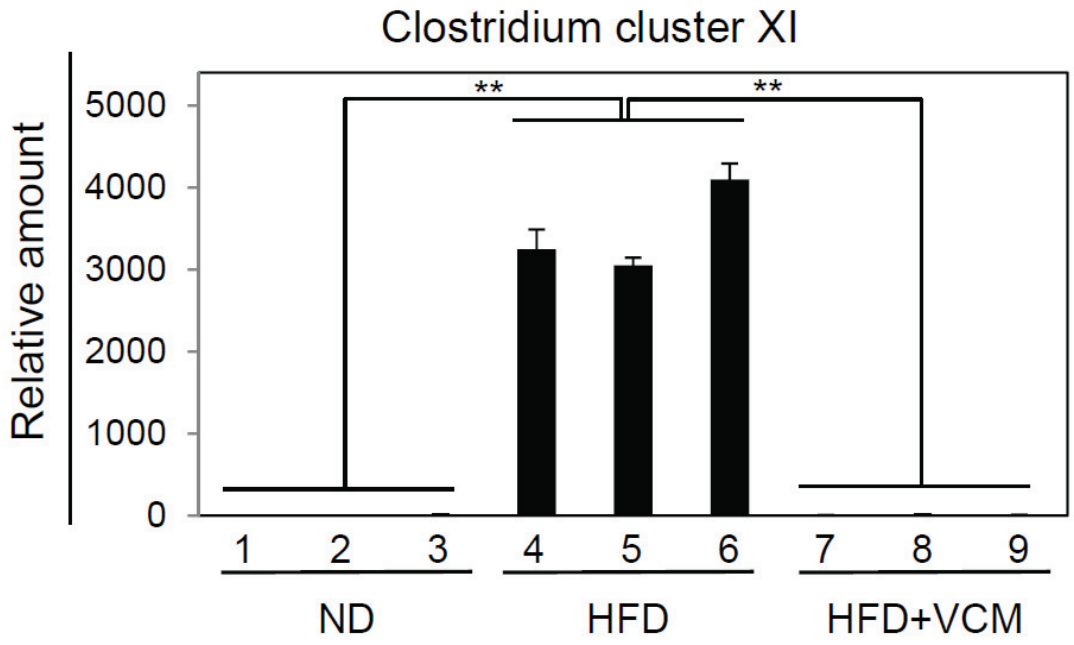

Supplementary Fig. 13| *Clostridium* cluster XI is associated with obesity-induced HCC development. The qPCR analysis of *Clostridium* cluster XI 16S rRNA gene in the feces (180mg) of indicated mice (n=3 per group). Error bars indicate mean ± s.d. ***P*<0.01.

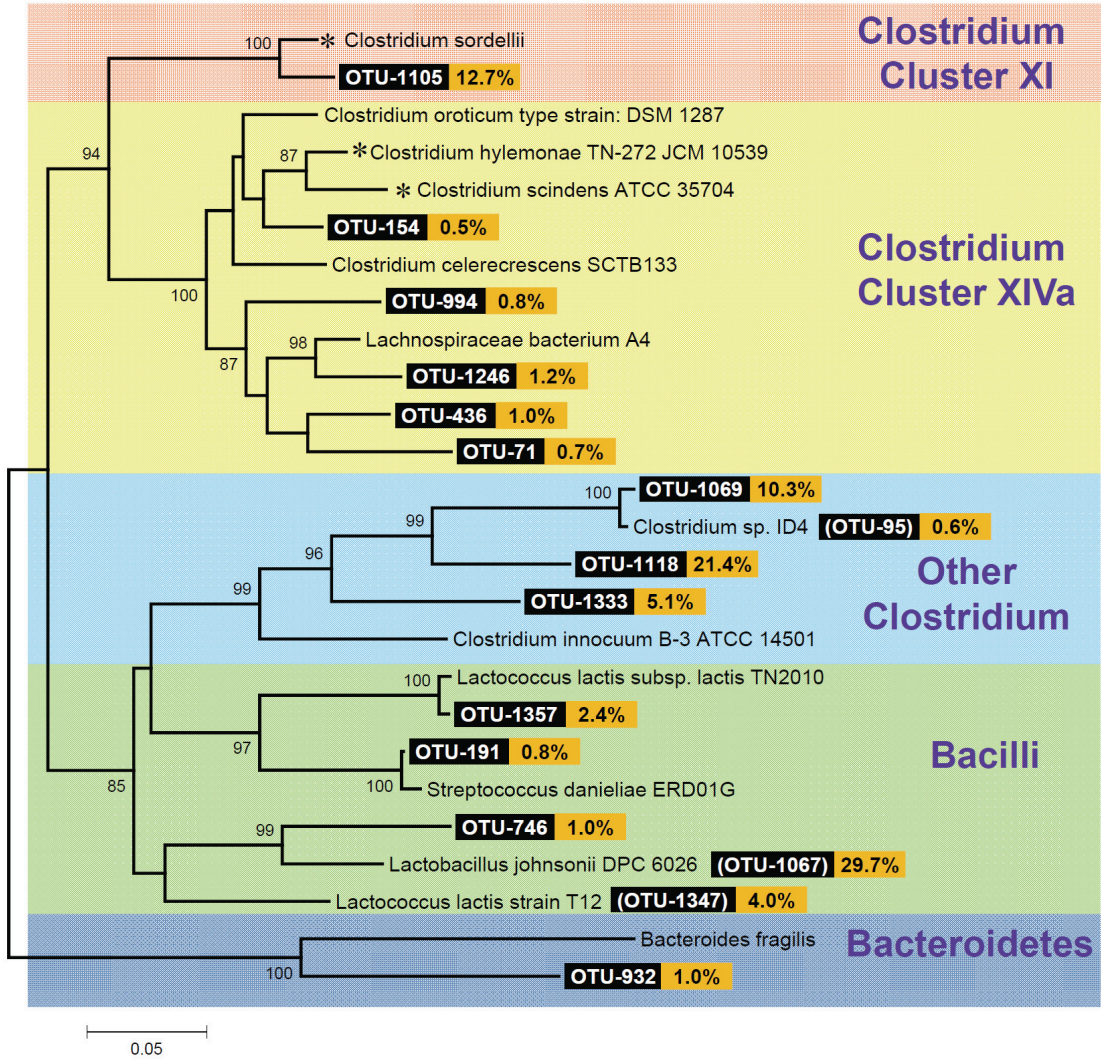

Supplementary Fig. 14| Phylogenetic analysis of fecal bacterial OTUs in HFD fed mice. Bacterial genomic DNA was isolated from faeces of HFD fed mice (see Figs.4a) and was subjected to amplification of hyper variable regions of the bacterial 16S rRNA gene using PCR, followed by pyrosequencing. Sequencing reads were quality filtered, de-multiplexed and assembled to construct OTUs by QIIME software with the cutoff similarity of 97% identity. A phylogenetic tree was constructed using neighbour-joining method with resulting sequences of obtained OTUs (white) and those of the closest strains in the database (black) using MEGA software[34]. Bacterial OTUs represent more than 0.5% of the fecal bacteria in HFD-fed mice are shown. * indicates bacterial strains known to possess DCA producing activity. Only bootstrap percentages greater than 80 are shown.

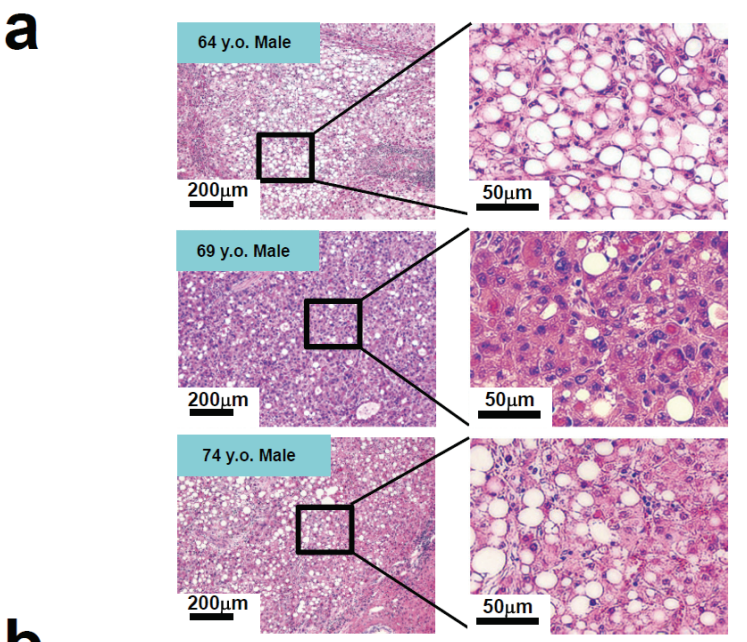
a
64 y.o. Male
200μm
50μm
69 y.o. Male
200μm
50μm
74 y.o. Male
200μm
50μm

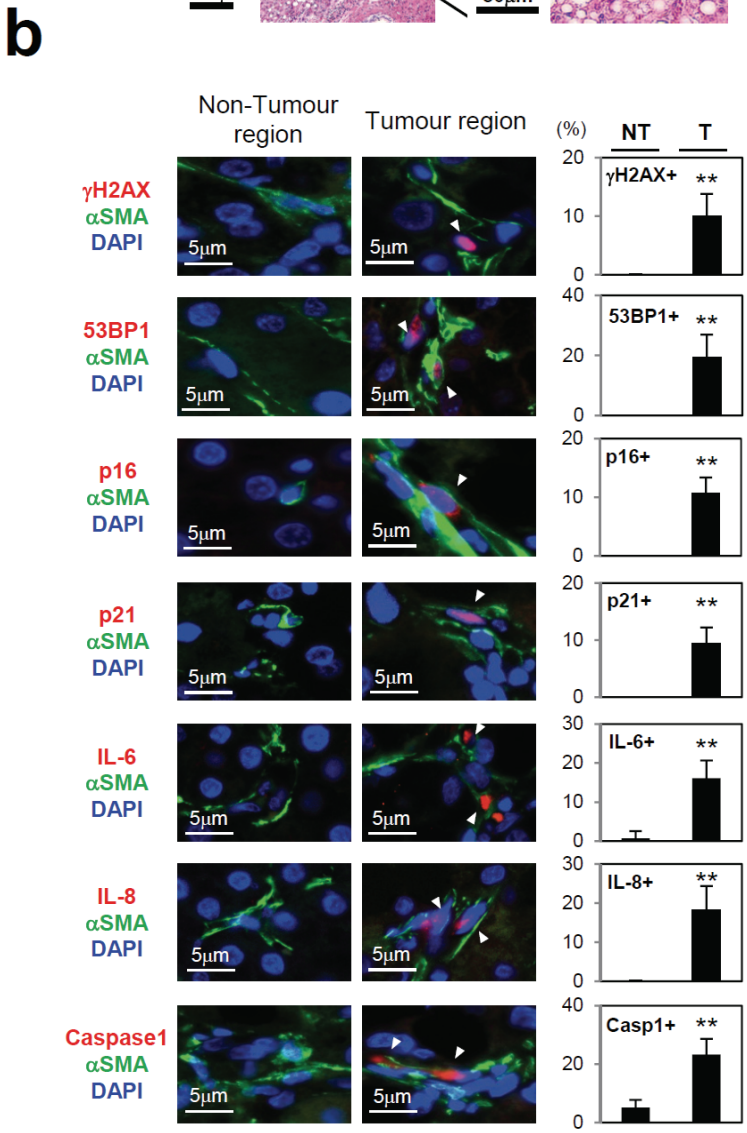
b
Non-Tumour region
Tumour region
(%)
NT
T
γH2AX
αSMA
DAPI
γH2AX+
53BP1
αSMA
DAPI
53BP1+
p16
αSMA
DAPI
p16+
p21
αSMA
DAPI
p21+
IL-6
αSMA
DAPI
IL-6+
IL-8
αSMA
DAPI
IL-8+
Caspase1
αSMA
DAPI
Casp1+
5μm
**

Supplementary Fig. 15| Cellular senescence and SASP in human HSCs in the area of HCC arising in patients with NASH. Paraffin embedded liver tissues of the patients with clinical and histological features of non-viral and non-alcoholic hepatocellular carcinomas resected in the Cancer Institute Hospital of JFCR (26 cases having Body-Mass Index higher than 25Kg/m^2) were examined. The H&E staining (**a**) and immunofluorescence analysis (**b**) of human liver cancers arising in patients with NASH are shown. These tumours were diagnosed as HCC with marked fatty change without apparent fibrosis. A series of senescence markers such as DNA damage response markers (γH2AX foci and 53BP1 foci), CDK inhibitors ($p16^{INK4a}$ and $p21^{Waf1/Cip1}$) and SASP factors (IL-6 and IL-8) were co-stained with α-SMA (arrow heads). The scale bars represent 5μm in immunofluorescence data. HSCs were visualized by α-SMA and DNA was stained by DAPI. The histograms indicate the percentages of α-SMA expressing cells that were positive for the indicated markers. At least 100 cells were scored per group. For all graphs, error bars indicate mean ± s.d. (n=3 per group). $^{**}P<0.01$.

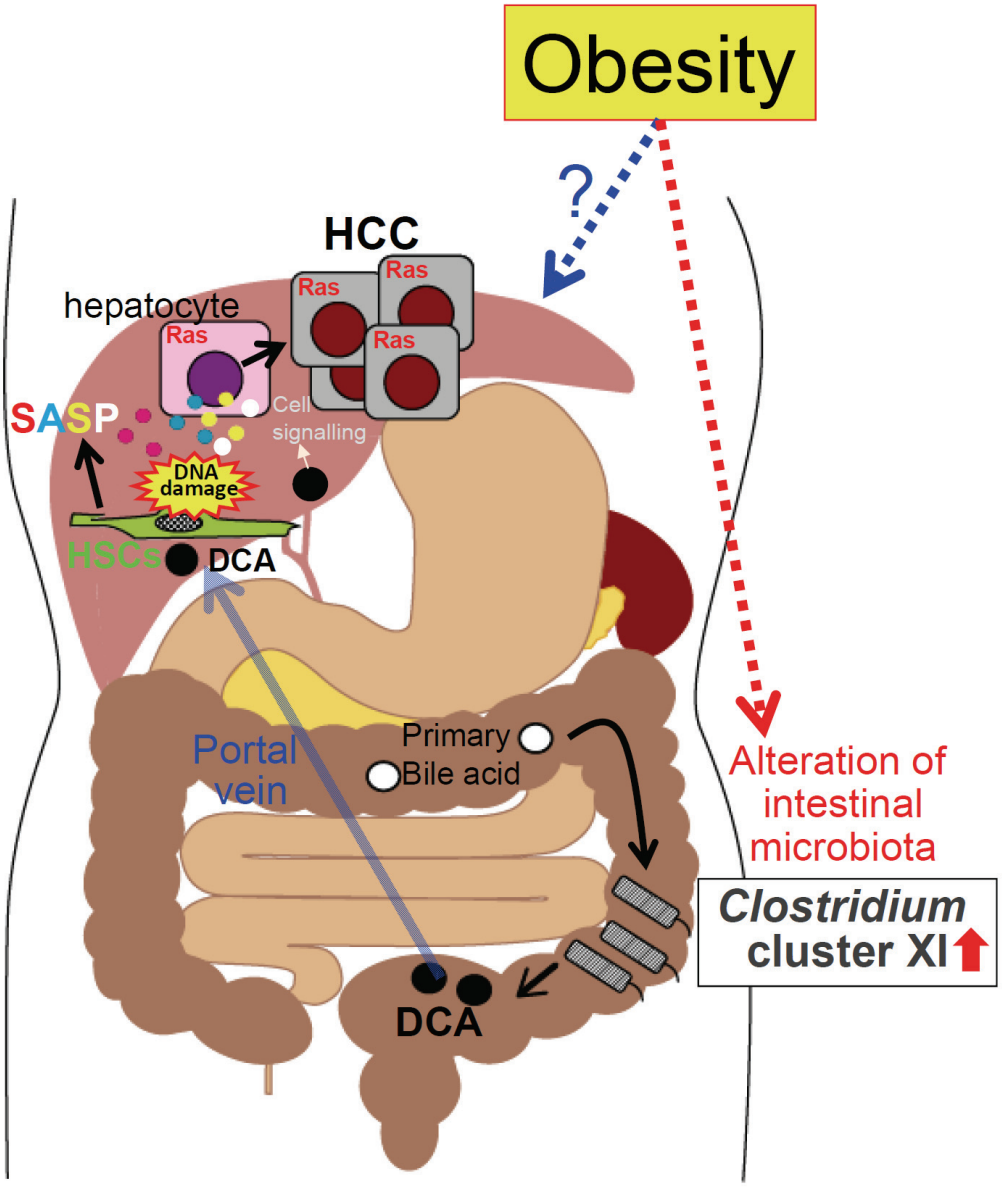

Supplementary Fig. 16| Model for obesity-induced HCC development *via* senescence secretome. Dietary or genetic obesity induces alteration of gut microbiota, thereby causing promotion of DCA production in intestinal tract. Elevated levels of DCA provoke SASP in HSCs through enterohepatic circulation, which in turn, secretes various inflammatory and tumour promoting factors in liver. This event, together with the activation of various cell signalling pathways (e.g. EGFR-pathway[40], ERK1/2-pathway[41], AKT-pathway[42] and β-catenin pathway[43]) by DCA, results in the promotion of HCC development.

2. Supplementary References

40. Qiao, L. *et al.* Deoxycholic acid (DCA) causes ligand-independent activation of epidermal growth factor receptor (EGFR) and FAS receptor in primary hepatocytes: inhibition of EGFR/mitogen-activated protein kinase-signaling module enhances DCA-induced apoptosis. *Mol. Biol.Cell* **12,** 2629-2645 (2001).
41. Cheng, K. & Raufman, J. P. Bile acid-induced proliferation of a human colon cancer cell line is mediated by transactivation of epidermal growth factor receptors. *Biochem. Pharmacol.* **70,** 1035-1047 (2005).
42. Fang, Y. *et al.* Bile acids induce mitochondrial ROS, which promote activation of receptor tyrosine kinases and signaling pathways in rat hepatocytes. *Hepatology* **40,** 961-971 (2004).
43. Pai, R., Tarnawski, A. S. & Tran, T. Deoxycholic acid activates beta-catenin signaling pathway and increases colon cell cancer growth and invasiveness. *Mol. Biol. Cell* **15,** 2156-2163 (2004).